Single-particle effects in precompound reactions: Influence of the $f_{7/2}$ shell closure

M. Blann, S. M. Grimes,* L. F. Hansen, T. T. Komoto, B. A. Pohl, W. Scobel,† M. Trabandt,† and C. Wong
Lawrence Livermore National Laboratory, University of California, Livermore, California 94550
(Received 16 April 1985)

We present angle integrated spectra for the (p,n) reaction with 25 MeV protons on targets of $^{50,52,53}_{24}$Cr, and on $^{58}_{26}$Fe, $^{59}_{27}$Co, $^{60}_{28}$Ni, and $^{63}_{29}$Cu. These spectra are compared with two-quasiparticle state densities for proton-particle—neutron-hole configurations, calculated using Nilsson-model single-particle energies. The influence of shell structure on the precompound spectra, previously shown for the $g_{9/2}$ neutron shell closure, is shown here for the $f_{7/2}$ neutron and proton shells. Semiquantitative agreement is shown between experimental results and calculated two-quasiparticle densities. The parameter space of pairing energy, deformation, and oscillator stiffness is explored. Precompound spectra near shell closures are in better agreement with partial state densities from Nilsson-model considerations than with results from more commonly used equidistant spacing models.

I. INTRODUCTION

This is the second of two reports[1] seeking to relate the gross structure of precompound decay spectra to few-quasiparticle state densities calculated incoherently from realistic single-particle levels. In most cases precompound spectra have been calculated in terms of partial state densities evaluated with an equidistant spacing assumption, guaranteeing that smooth, structureless spectra will be the result of any model calculation. Yet it was pointed out at an early stage of precompound model development that structure might be expected to persist in precompound spectra populating quite high excitations when the irregular spacing of realistic single particle levels was considered.[2,3] Some early attempts to verify such shell effects were made on existing spectra,[4] but experiments designed to optimize success of this quest were not specifically undertaken or reported. With this in mind we have measured (p,n) spectra on a sequence of targets selected to show the effects of shell closures on precompound decay spectra; we then compare the experimental results with $(p)(n)^{-1}$ (i.e., one proton particle, one neutron hole) two-quasiparticle densities of the residual nucleus after neutron emission calculated with single particle levels from Nilsson models with different parametrizations.

Our experiments were performed with 25 and 18 MeV protons from the Lawrence Livermore National Laboratory (LLNL) cyclograaff accelerator. In an earlier work we reported results of (p,n) spectra on $^{90,91,92,94}_{40}$Zr targets, and analyses of these spectra in terms of two-quasiparticle partial state density calculations.[1] The latter probed the degree of structure generated in neutron spectra where the $g_{9/2}$ neutron shell closure was expected to have a large influence. In the present work we present (p,n) spectra on $^{50,52,53}_{24}$Cr, $^{54,56,58}_{26}$Fe, $^{59}_{27}$Co, $^{60}_{28}$Ni, and $^{63}_{29}$Cu with 25 MeV protons. These targets allow us to probe the influence of the $f_{7/2}$ neutron and proton shell closures on the precompound spectra, and allow us to test the realistic partial state density model over a broader range of nuclei than in Ref. 1, providing a broader base on which to conclude the efficacy of the simple approach used, and to decide if more sophisticated models are warranted.

The experimental methods used were presented in Ref. 1, as were details of the calculations. We therefore give a very brief discussion of these points in the present work. In Sec. II we give a brief summary of the experimental method. In Sec. III we discuss the manner in which shell effects should influence the (p,n) precompound decay spectra, and describe the basis for a comparison of model calculations including realistic state densities with experimental neutron energy spectra. In Sec. IV we compare results of such calculations with our experimental data, with conclusions summarized in Sec. V.

II. EXPERIMENTAL METHODS

The experiments were performed using the LLNL cyclograaff accelerator facility for production of a 25.0 ± 0.08 MeV proton beam. Neutrons were detected with a 16 detector array spanning the angular range 3.5° to 159°. The target thickness, isotopic abundances, and accumulated charges for measurements reported in this work are summarized in Table I, the reaction data in Table II, of Ref. 1.

The neutron time-of-flight (TOF) setup consisted of 10×5 cm NE213 detectors behind flight paths of 10.7 m length. The burst repetition rate was 2.5 MHz. The overall time resolution of 1.0—1.5 ns allowed for an energy resolution $\Delta E\approx300$ keV at $E_n\approx20$ MeV. Measurements were performed with metallic target foils of 2.3—5.4 mg/cm^2 thickness. Each run was supplemented by a background run with an empty target frame yielding a correction of typically $\lesssim10\%$. Angle integrated spectra can be followed down to the 100 μb/MeV level; we estimate uncertainties $\lesssim15\%$ for most of the double differential and $\lesssim11\%$ for the angle integrated differential cross sections. These numbers may be higher for the low neutron yield reactions p + ^{50}Cr,^{54}Fe at the highest possible neutron energies. All data presented here are for isotopically pure targets. The corrections for isotopic admixtures were possible because we measured the (p,n) reaction for all relevant isotopes such that the energy spectra could be unfolded consistently, in particular for ^{58}Fe with its

low (0.34%) natural abundance.

A more detailed report on experimental details may be found in Ref. 1; the numerical tables of all double differential and angle integrated data are also available.[5]

III. PREEQUILIBRIUM EMISSION AND SHELL MODEL BASED PARTIAL STATE DENSITIES

A. Qualitative expectations of spectral effects

In Fig. 1 we show the particle occupations with neutrons for $^{50}_{24}$Cr, $^{52}_{24}$Cr, and $^{53}_{24}$Cr in single-particle level diagrams around the $f_{7/2}$ shell closure. In Fig. 2 we show a similar diagram for proton levels for $^{58}_{26}$Fe, $^{59}_{27}$Co, and $^{60}_{28}$Ni. The single particle levels shown were generated with a Saxon-Woods potential shape using parameters of Kisslinger and Sorenson.[6] It is worthwhile to explore some qualitative expectations for the (p,n) spectra with respect to the simple diagrams of Figs. 1 and 2 before making more quantitative comparisons with two-quasiparticle state density calculations.

We consider the $(p)(n)^{-1}$ (proton-particle, neutron-hole) state density of the residual nucleus because precompound decay models predict that the main contribution to the spectrum comes from decay of the first collisional excitations, which for nucleon-induced reactions in an extreme two body transition model creates two-particle—one-hole excitations.[7] For a proton-induced reaction in which a neutron is to be emitted, only $(p)(n)(n)^{-1}$ configurations will be of interest. The residual nuclei will be $(p)(n)^{-1}$, and the density of states of the $(p)(n)^{-1}$ configurations at a given residual excitation energy according to Fermi's golden rule is related to the probability of emitting a neutron leading to that residual excitation.

Consider the sequence of target isotopes ^{50,52,53}Cr in Fig. 1.[6] A ground state transition may result when the incident proton strikes any of six degenerate $f_{7/2}$ neutrons in ^{50}Cr, or any of eight neutrons in ^{52}Cr. In each case the proton may populate any of four vacant $f_{7/2}$ orbitals in a reaction populating the ground state. One therefore expects a reasonably strongly populated ground state transition in the (p,n) spectra on either target. Consider next ^{53}Cr. Here the ground state results only if the incident proton reacts with the lone $p_{3/2}$ neutron. More highly excited final states will be formed only when a neutron from the $f_{7/2}$ level (or deeper) is excited, and this will require at least 4 MeV of energy corresponding to the $f_{7/2}$-$p_{3/2}$ energy difference. Comparisons of the (p,n) spectra on the ^{50,52,53} Cr isotopes should therefore test the influence of the $f_{7/2}$ shell gap on the precompound neutron spectra. (The case is a bit more complicated due to the fact that the isobaric analog resonance coincides with the g.s. of the residual nucleus ^{50}Mn and is at only 2.93 MeV excitation in ^{51}Mn.)

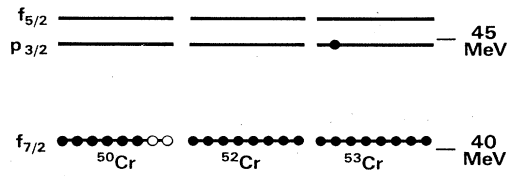

FIG. 1. Diagram of particles and holes at the top of the Fermi sea for neutrons in ^{50}Cr, ^{52}Cr, and ^{53}Cr. The influence the nuclear structure is expected to have on the precompound spectra is discussed in the text. Closed circles represent filled neutron levels; open circles or blanks represent holes.

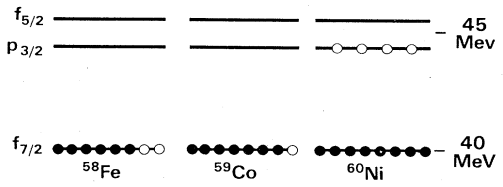

FIG. 2. Diagram of the proton particle and hole occupation at the top of the Fermi sea for protons in ^{58}Fe, ^{59}Co, and ^{60}Ni. Symbols are as in Fig. 1.

The influence of the proton orbitals on precompound spectra should be visible by comparing (p,n) spectra from the $^{58}_{26}$Fe,$^{59}_{27}$Co,$^{60}_{28}$Ni sequence illustrated in Fig. 2. The ground state of the residual nucleus may be formed by ex-

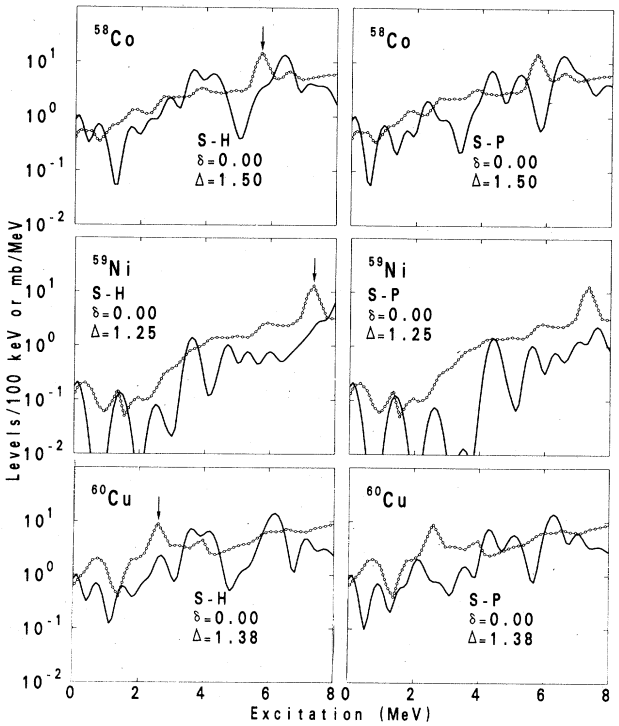

FIG. 3. Experimental angle integrated (p,n) spectra versus residual excitation for reactions of 25 MeV protons on ^{58}Fe, ^{59}Co, and ^{60}Ni, and calculated $(p)(n)^{-1}$ partial state densities for the respective residual nuclei. The connected open dots represent experimental results; the line represents the calculation. The pairing energies Δ are slightly varied from those given in Ref. 15; spherical nuclei were assumed; single particle levels from Seeger-Howard (Ref. 11) (S-H) and Seeger-Perisho (Ref. 12) (S-P) were used in the calculations. Downward arrows indicate positions of the isobaric analog ground state.

citing one of the four $p_{3/2}$ neutrons in any of these targets. The proton may go into either of two vacant $f_{7/2}$ orbitals for the ^{58}Fe target, and it may go into only a single vacant $f_{7/2}$ orbital for the ^{59}Co target. However, for the ^{60}Ni target the proton may go into any of the four vacant $p_{3/2}$ orbitals in populating the ground state. We therefore expect a small g.s. transition on ^{58}Fe, smaller on ^{59}Co, and then a very much stronger g.s. transition with the ^{60}Ni target. Because $f_{5/2}$ excited proton orbitals are near the $p_{3/2}$ g.s. in ^{60}Ni, versus requiring the $f_{7/2}$-$p_{3/2}$ energy difference in ^{58}Fe and ^{59}Co targets, we expect a rapid increase of excited levels (on emission neutron intensity) with energy for the ^{60}Ni target as compared with the ^{59}Co and ^{58}Fe results. These qualitative features are generally supported by the experimental angle integrated (p,n) spectra shown in Fig. 3. In the following section we discuss the more difficult question of semiquantitative comparisons between the experimental spectra and $(p)(n)^{-1}$ state densities calculated with shell model single particle energies.

B. Energy spectra and partial state densities

Nucleon energy spectra due to prevailing preequilibrium emission can be described with semiclassical models like the exciton or the hybrid model.[7] The gross features of these models can be expressed[8] in one equation valid for both of them, viz.,

$$\frac{d\sigma(\epsilon_\nu)}{d\epsilon_\nu}=\sigma_R(\epsilon_a)\sum_{n=n_0}^{\bar{n}} D_n P_n(\epsilon_\nu+B_\nu,E) \times\lambda_c(\epsilon_\nu)t(n,\epsilon_\nu,E)\ , \tag{1}$$

where σ_R denotes the reaction cross section leading to a system with excitation E. The sum extends over contributions of stages characterized by the exciton number $n=p$ (particles) + h (holes); λ_c is the decay rate for the continuum emission of nucleons of type ν, energy ϵ_ν, and separation energy B_ν; D_n is the depletion due to this emission from preceding stages $n'<n$. The models differ in the lifetime expression $t(n,\epsilon_\nu,E)$, but apply the same nucleon density distributions

$$P_n(\epsilon_\nu+B_\nu,E)=g\frac{\rho_{p-1,h}(U)}{\rho_n(E)}\ , \tag{2}$$

where $U=E-\epsilon_\nu-B_\nu$ and ρ denotes the density of states with the indicated excitation and exciton configuration.

Inspection of Eqs. (1) and (2) reveals[1] that, due to the dominance of the leading term in the sum, the dependence on ϵ_ν is given in first order by

$$\frac{d\sigma(\epsilon_\nu)}{d\epsilon_\nu}\sim\rho_{p-1,h}(U)\ . \tag{3}$$

For (p,n) reactions, the residual nucleus is left at this stage ($n=n_0=3$) in a $(1p)(1n)^{-1}$ state.

Equation (3) has been used in Ref. 1 as basis for a comparison of experimental spectra with different approaches for the partial state density on the right-hand side. Partial state densities can be calculated from a set of single particle energies by the recursion relation of Refs. 2 and 9. For equidistantly spaced single particle levels this recursion yields the well-known Ericson result,[10] a smooth function of energy U. However, the recursion relation may also be applied to any given set of single particle energies that can be generated as a function of the nucleide mass A, the number of fermions (N or Z), and a deformation parameter δ.

IV. COMPARISON OF (p,n) SPECTRA WITH REALISTIC TWO-QUASIPARTICLE DENSITIES

We will first compare quasiparticle densities generated using single particle levels of Seeger and Howard[11] and of Seeger and Perisho.[12] After an exploration of the effects of changing pairing, deformation, and oscillator stiffness parameters with these single particle sets, we will make additional comparisons using single-particle levels generated using a deformed Woods-Saxon potential with parameters of Kisslinger and Sorensen.[6]

The state density code used[1] converts single particle energies to quasiparticle energies with the formalism of Bardeen, Cooper, and Schrieffer.[13] This way pairing effects can be introduced via the gap parameter Δ. The neutron and proton state densities are folded with a Gaussian function to give finite linewidths. We have used an averaging width parameter of 1.5 MeV for all results to be presented in this work. There were a number of caveats presented in Ref. 1 as to why we should not expect too much of these calculations, and suggestions were made on how the calculations may be improved in the future. We repeat those points here:

(1) The calculation considers only the energies of the single particle levels; however, each residual interaction and coupling of the angular momenta of unpaired particles should yield different level energies rather than the degenerate results assumed in our codes.

(2) The targets used, due to being closed shell or near-closed shell in nature, involve single particle orbitals which may have very large ranges of angular momenta to which they may couple. The centrifugal barrier may strongly inhibit population of some of these levels due to the kinematically allowed orbital angular momentum transfers. These restrictions are not considered (as yet) in comparing data with results of our codes for generating few quasiparticle densities.

(3) Positions calculated for excited single particle levels will be even more sensitive to details of the shape of the assumed potential well than for lower lying orbitals.

(4) As particle orbitals become unbound, the interpretation of shell model levels becomes ambiguous; the centrifugal barrier, and for protons the Coulomb barrier, may mitigate this point for a few MeV. For isotopes of interest in this work, the proton binding energies are as low as 3 MeV (^{60}Cu), and generally are around 8 MeV.

(5) As the single particle energies increase, the lifetime decreases, and the natural width due to the Heisenberg uncertainty principle increases. Similarly, the spreading width will change. We might therefore expect that the

constant averaging width of our calculation might better be replaced by an energy dependent function, which would smooth the structure at higher excitations. Contributions from four-quasiparticle states would also do this.

(6) The excited nuclei, which may have high ($\approx 8\hbar$) angular momenta, may have deformations larger than the ground state target nuclei.[14]

Having stated the major shortcomings of the calculated few-quasiparticle densities, we proceed to make comparisons with experimental spectra. To do so we apply Eq. (3) to the residual excitation spectra $d\sigma(E-B_n-\epsilon_n)/d\epsilon_n$ and the two-quasiparticle state densities calculated with the code of Williams *et al.*[2] as modified by Albrecht[3] and by Grimes.[4]

Results for the target sequence ^{58}Fe,^{59}Co,^{60}Ni, leading to residual nuclei ^{58}Co, ^{59}Ni, and ^{60}Cu, are shown in Fig. 3. Pairing energies Δ were varied from initial choices based on the work of Gilbert and Cameron[15] for this and the following figures. Spherical nuclei were assumed, and results are shown for both Seeger-Howard[11] and Seeger-Perisho[12] single particle levels. The small ground state transition followed by a gap, qualitatively predicted in the preceding section and seen in the data for ^{59}Co(p,n), is also reproduced by the calculated two-quasiparticle densities. There is also some agreement in the energies of the low lying peaks, and in the general envelope (by which we mean a smooth line drawn through the spectra, averaging out level structure) versus excitation.

For the residual nucleus ^{58}Co, the lessening of the low energy gap as compared to ^{59}Ni due to the incompletely filled $f_{7/2}$ proton shell and the resulting spreading of single particle (s.p.) strength is seen. The low energy gap disappears for the residual nucleus ^{60}Cu both for experiment and calculation; the latter shows sharper structures due to the assumed sphericity; cf. Fig. 3. For both cases we can state reasonable agreement between experiment and calculation, in particular if the structures of the partial state densities are smoothed.

In Fig. 4 we demonstrate for ^{60}Cu the effects of varying

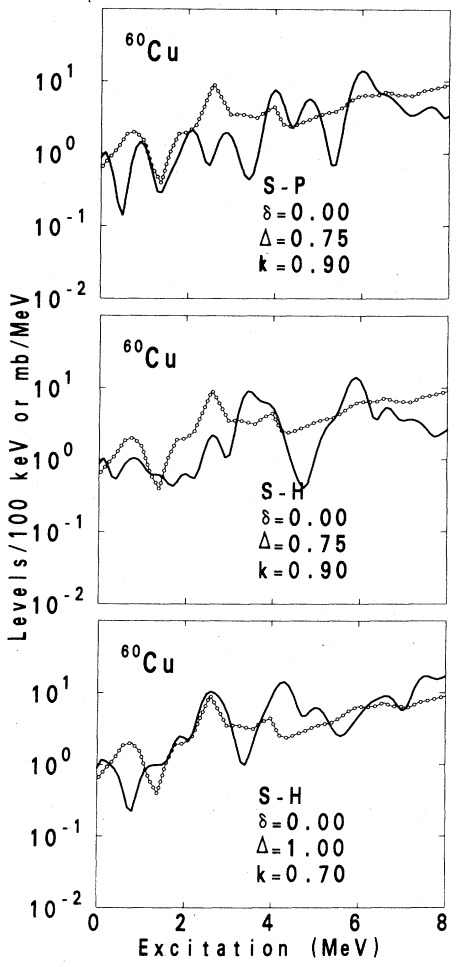

FIG. 4. Experimental angle integrated neutron spectra and calculated $(p)(n)^{-1}$ partial state densities for the (p,n) reaction on ^{60}Ni. Line types as in Fig. 3. The single particle level set and pairing strength are indicated in the figure. Spherical nuclei were assumed. The k value multiplies the constant of the oscillator stiffness, $\omega = A/(\text{const} \times k)$; pairing values were selected arbitrarily to improve agreement with low lying experimental structure.

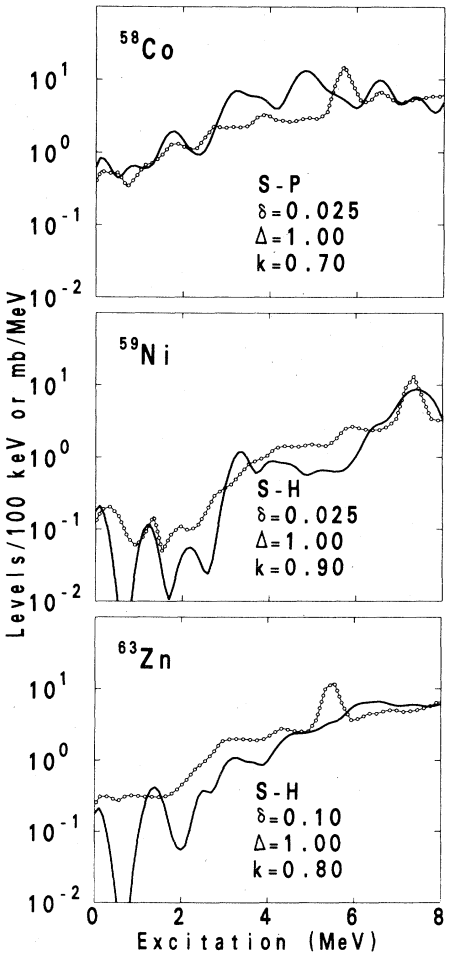

FIG. 5. Experimental neutron spectra and calculated $(p)(n)^{-1}$ partial state densities for the (p,n) reaction on ^{58}Fe, ^{59}Co, and ^{63}Cu, and for the residual nuclei ^{58}Co, ^{59}Ni, and ^{63}Cu. Line types are as in Fig. 3. The parameter sets used are indicated in the figure. Calculations were for slightly deformed nuclei.

the oscillator stiffness $\omega = A/\text{const}$ by multiplication of the denominator with the value k, on choice of the single particle set, and on the pairing correction $\Delta_n = \Delta_p = \Delta$. The influence of Δ is smaller for the odd-odd nucleus than for the odd-even nucleus as expected, whereas $k \neq 1$ considerably varies the detailed structure of the $(1p)(1n)^{-1}$ state density. In Fig. 5 we show the effects of varying oscillator stiffness, slightly varying the pairing force, and adding a small amount of quadrupole deformation δ to the Nilsson[16] potential. In Fig. 5 we have also shown a ^{63}Zn residual nucleus comparison; while this adds one more ground state proton to the Co-Ni-Cu sequence, the neutron number is different. Here too the general envelope of the shell model based few-quasiparticle density of states agrees reasonably well with the experimental spectrum. The ^{58}Co and ^{59}Ni calculated spectra also agree reasonably well with the experimental results. In these and the following figures the parameter choices have been made on an arbitrary basis in order to give some optimization of agreement with experimental results. Our goal is to demonstrate that reasonable parameters give reasonable agreement. We are not in a position to calculate the best possible agreement on an *a priori* basis.

Similar comparisons testing the $f_{7/2}$ neutron shell, rather than the $f_{7/2}$ proton shell, are shown in Fig. 6 for the ^{50,52,53}Mn residual nuclei. The low energy gap predicted qualitatively for ^{53}Mn is reproduced quite well in the calculated spectra, with reasonable agreement in peak positions for low lying excitations. The oscillator stiffness was varied from the Seeger-Howard/Seeger-Perisho values as indicated, and the pairing strengths were taken to be lower than the Gilbert-Cameron values to improve the agreement of low lying levels. For the Seeger-Howard single particle set a small deformation was also used.

In Figs. 7–9 we show results for the ^{58}Co,^{59}Ni,^{60}Cu nuclei, ^{50,52,53}Mn nuclei, and ^{90,91,92,94}Nb nuclei, all calculations having been performed with single particle levels calculated in a deformed Woods-Saxon potential, with parameters (including pairing) from the work of Kisslinger and Sorensen,[6] all with a deformation parameter $\beta_2 = 0.1$. No attempt has been made to empirically optimize these results.

The general envelopes of the calculated results in Figs. 7–9 are in general agreement with the experimental trends. Specific peaks are not in particularly good agreement, nor have pairing and deformation parameters been varied to improve agreement. However, for all cases presented in Figs. 3–9, the general envelopes of the exper-

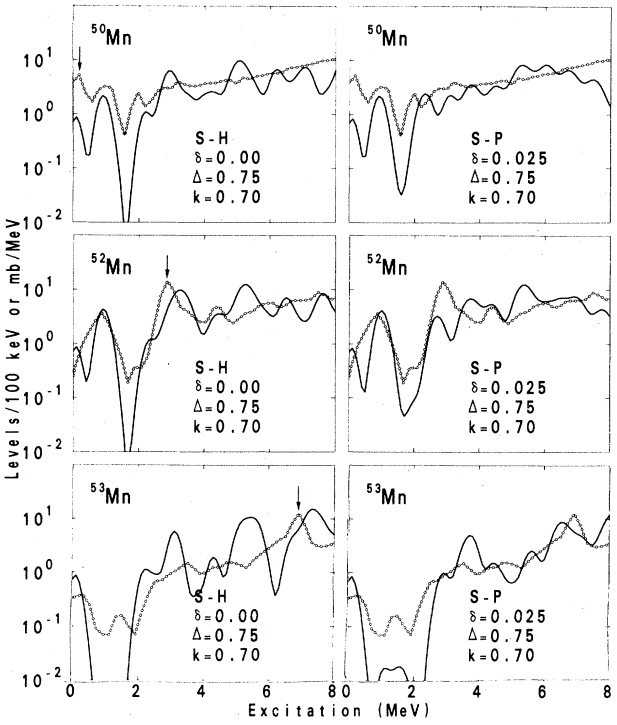

FIG. 6. Experimental neutron spectra and calculated $(p)(n)^{-1}$ partial state densities for the (p,n) reaction on ^{50,52,53}Cr and for the resulting residual nuclei ^{50,52,53}Mn. The line types are as in Fig. 3. The parameter sets used are indicated in the figure. Downward arrows indicate positions of the isobaric analog ground state.

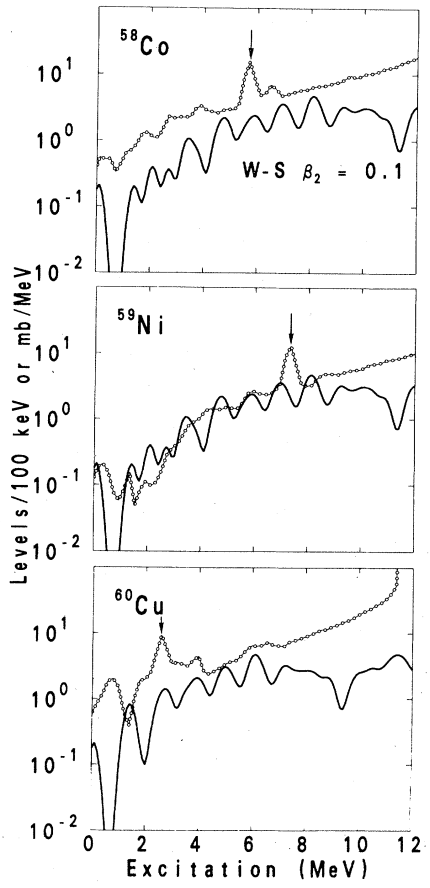

FIG. 7. Experimental neutron spectra and calculated $(p)(n)^{-1}$ partial state densities for the (p,n) reaction on ^{58}Fe, ^{59}Co, and ^{60}Ni leading to ^{58}Co, ^{59}Ni, and ^{60}Cu residual nuclei. Line types are as in Fig. 3. The calculated results all use the Woods-Saxon single particle levels of Kisslinger and Sorensen (Ref. 7) with a deformation parameter of $\beta_2 = 0.1$, and pairing strength based on values given or extrapolated from Ref. 6.

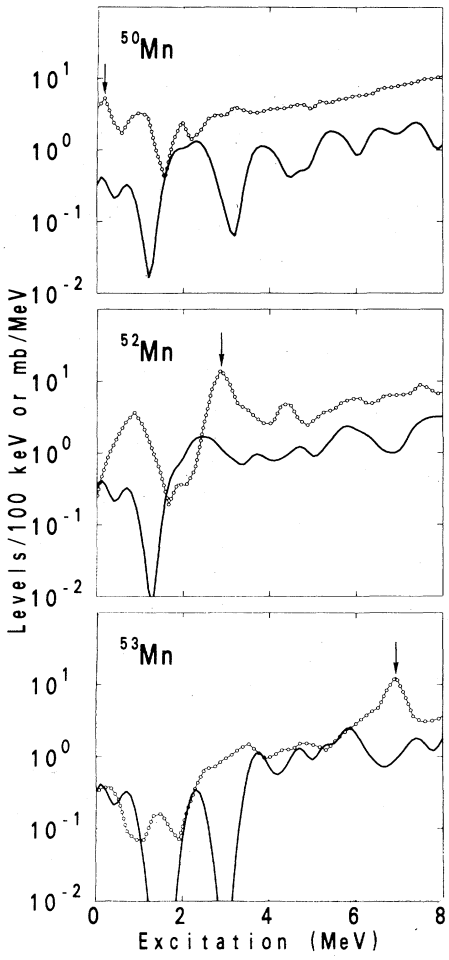

FIG. 8. Experimental neutron spectra and calculated $(p)(n)^{-1}$ partial state densities for (p,n) reactions giving the residual nuclei ^{50,52,53}Mn. Line types are as in Fig. 3. Calculations are as for Fig. 7.

imental spectra are reproduced better with shell model generated $(p)(n)^{-1}$ state densities than with the more common equidistant model results used in precompound decay calculations. The large shell effects observed in the experiments and confirmed in the calculations indicate that precompound calculations employing an equidistant quasiparticle (exciton) density expression with a simple pairing treatment are doomed to failure in predicting low lying populations near shell closures. The shell effect may be seen to be considerably larger than pairing effects in the shell closure regions.

V. CONCLUSIONS

The large shell effects observed in precompound spectra for nuclei around the $g_{9/2}$ neutron shell closure[1] are also seen for the $f_{7/2}$ neutron and proton shells. Shell model calculations for the $(p)(n)^{-1}$ configurations, which should be of major importance in the low lying (below 8 MeV) excitations populated in the (p,n) experiments performed, generally reproduce the main envelopes of the experimental results. There is some ability also to calculate the positions of peaks in the spectra at quite low excitations that are sensitive to modest variations of the shell model parameters. The shell model results will be more meaningful when the partial state densities are calculated versus angular momentum; it will then be possible to exclude excitations which require more angular momentum than the incident and emitted nucleons (coupled to target spin) can

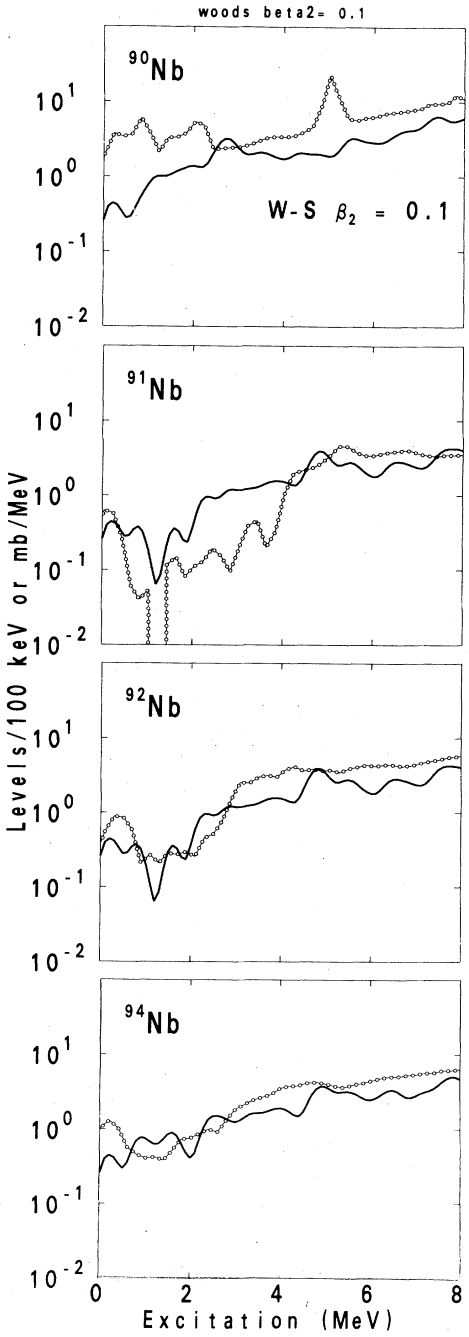

FIG. 9. Experimental neutron spectra and calculated $(p)(n)^{-1}$ partial state densities for (p,n) reactions giving the residual nuclei ^{90,91,92,94}Nb. Data are from Ref. 1. Calculations are as in Fig. 7.

account for. When angular momentum can be treated at least crudely, it may be worthwhile to couple the few-quasiparticle density code to a least squares search routine to seek single particle levels giving a "best fit" to experimental spectra. We expect the two-body interaction will in general spread and shift single particle state centroids. Results such as the present measurements, when compared with calculations including angular momentum, should improve our understanding of the relative importance of these two effects. The (p,n) reaction should preferentially excite $(p)(n)^{-1}$ configurations; (n,n') should populate $(n)(n)^{-1}$ and $(p)(p)^{-1}$ configurations, etc. We then may have a tool for probing centroids of microscopic aspects of highly excited states.

ACKNOWLEDGMENTS

Two of us (W.S and M.T.) appreciate the hospitality at LLNL and acknowledge partial support from the Bundesministerium für Forschung und Technologie. This work was performed under the auspices of the U.S. Department of Energy by the Lawrence Livermore National Laboratory under contract number W-7405-ENG-48.

---

*Permanent address: Ohio University, Athens, OH 45701.
†Permanent address: Universität Hamburg, D-2000 Hamburg, Federal Republic of Germany.

[1]W. Scobel *et al.*, Phys. Rev. C **30**, 1480 (1984).
[2]F. C. Williams, Jr., A. Mignerey, and M. Blann, Nucl. Phys. **A207**, 619 (1973).
[3]K. Albrecht and M. Blann, Phys. Rev. C **8**, 1481 (1973).
[4]S. M. Grimes, J. D. Anderson, and C. Wong, Phys. Rev. C **13**, 2224 (1976); C. Wong, J. D. Anderson, J. C. Davis, and S. M. Grimes, *ibid.* **7**, 1895 (1973).
[5]W. Scobel *et al.*, Lawrence Livermore National Laboratory Report No. UCID-20101, 1984 (unpublished).
[6]L. S. Kisslinger and R. A. Sorensen, Rev. Mod. Phys. **35**, 853 (1963).
[7]M. Blann, Annu. Rev. Nucl. Sci. **25**, 123 (1975).
[8]J. Ernst and J. Rama Rao, Z. Phys. A **281**, 129 (1977).
[9]F. C. Williams, Nucl. Phys. **A133**, 33 (1969).
[10]T. Ericson, Adv. Phys. **9**, 425 (1960).
[11]P. A. Seeger and W. M. Howard, Nucl. Phys. **A238**, 491 (1975).
[12]P. A. Seeger and R. C. Perisho, Los Alamos National Laboratory Report No. LA3751, 1967 (unpublished).
[13]J. Bardeen, L. N. Cooper, and J. R. Schrieffer, Phys. Rev. **108**, 1175 (1957); L. G. Moretto, Nucl. Phys. **A182**, 641 (1972); S. M. Grimes, in *Theory and Application of Moment Methods in Many Fermion Systems,* edited by B. J. Dalton, S. M. Grimes, J. P. Vary, and S. A. Williams (Plenum, New York, 1979), p. 17.
[14]S. Åberg, Phys. Scr. **25**, 23 (1982).
[15]A. Gilbert and A. G. W. Cameron, Can. J. Phys. **43**, 1446 (1965).
[16]S. G. Nilsson, K. Dan. Vidensk. Selsk. Mat.-Fys. Medd. **29**, No. 16 (1955).